

## Optical fluorescence excitation spectra of flux-grown stoichiometric europium vanadate crystals

R L Cone†, P C Hansen, M J M Leask and B M Wanklyn  
Clarendon Laboratory, Parks Road, Oxford OX1 3PU, UK

Received 1 October 1992

**Abstract.** The intrinsic site optical absorption of  $\text{EuVO}_4$  from  ${}^7\text{F}_0$  to  ${}^5\text{D}_0$ ,  ${}^5\text{D}_1$ ,  ${}^5\text{D}_2$ , and  ${}^5\text{D}_3$  exhibits normal behaviour, but sensitive laser excitation profiles measured in the  $\text{Eu}^{3+}: {}^7\text{F}_0 \rightarrow {}^5\text{D}_0$  region (580 nm) map out more than 40–50 defect lines spread over some  $60 \text{ cm}^{-1}$ . Each of these must be due to a distinct type of defect site in the crystal structure. A number of different  $\text{EuVO}_4$  crystals prepared from fluxes with different compositions have been used to show that some of these point defects are associated with specific chemical impurities while others seem to be present even in the purest crystals. Electronic Zeeman shifts of the  $\text{Eu}^{3+}: {}^7\text{F}_0 \rightarrow {}^5\text{D}_0$  optical lines for some of the low-symmetry perturbed sites provide additional information on defect geometry and on the low-lying  ${}^7\text{F}_1$  electronic levels for those specific perturbed sites. High degrees of site distortion are indicated for some of the sites, and principal axes are shown to make oblique angles to normal crystal axes.

### 1. Introduction

In a previous study of stoichiometric europium vanadate  $\text{EuVO}_4$  (Cone *et al* 1984), optical hole burning techniques were used to investigate crystallographically perturbed (defect) sites in high-quality single crystals. Optical absorption in the  $\text{Eu}^{3+}: {}^7\text{F}_0 \rightarrow {}^5\text{D}_0$  region (580 nm) showed more than fifty lines spread over some  $60 \text{ cm}^{-1}$ . Each of these extra lines could be ascribed to a distinct type of defect site in the crystal, since the  ${}^7\text{F}_0 \rightarrow {}^5\text{D}_0$  transition, being  $J = 0$  to  $J = 0$ , has no crystal field splittings. The  $\text{EuVO}_4$  crystals had been prepared using techniques of flux growth described in detail by Smith and Wanklyn (1974). A basic flux containing vanadium and oxygen was necessary, and initially this had been provided by a mixture of  $\text{Pb}_2\text{V}_2\text{O}_7$  and  $\text{V}_2\text{O}_5$ .

The present work is a thorough survey of twelve different batches of  $\text{EuVO}_4$  crystals prepared using several different fluxes and intentional dopings. The observed  $\text{Eu}^{3+}$  spectra are found, as expected, to depend on the particular flux used, but also to show a remarkable degree of uniformity. Many  $\text{Eu}^{3+}$  lines are observed in all of the  $\text{EuVO}_4$  preparations, while others appear only when the flux contains fluoride compounds, for instance. These and other features allow some conclusions to be drawn regarding the origin of defect sites in these  $\text{EuVO}_4$  crystals.

The present work also describes the most complete investigation so far of the spectroscopic properties of  $\text{Eu}^{3+}$  ions at the 'intrinsic' crystal sites in  $\text{EuVO}_4$ , that is, at the  $\text{Eu}^{3+}$  sites having the  $\text{D}_{2d}$  symmetry characteristic of the perfect crystal structure. For such sites the  ${}^7\text{F}_0 \rightarrow {}^5\text{D}_0$  transition is strictly forbidden and is

† Permanent address: Department of Physics, Montana State University, Bozeman, MT 59717, USA.

therefore not observed at all. The many lines observed in the  ${}^7F_0 \rightarrow {}^5D_0$  region are necessarily related to defect sites at which the lower crystallographic symmetry allows this transition to some extent. The transitions  ${}^7F_0 \rightarrow {}^5D_1, {}^5D_2, {}^5D_3$  are, on the other hand, strongly allowed for the intrinsic sites, and the spectra in these wavelength regions are thus dominated by the intrinsic site transitions, which are far more intense than the transitions originating at the defect sites as a result of simple number density comparisons for the sites. Detailed analysis of Zeeman spectra in these  ${}^7F_0 \rightarrow {}^5D_1, {}^5D_2, {}^5D_3$  regions shows that the  $\text{Eu}^{3+}$  intrinsic site behaviour is well understood in  $\text{EuVO}_4$ , an essential preliminary to any attempt at the analysis of defect site behaviour.

In other papers (Cone *et al* 1992, Sun *et al* 1993), the  ${}^7F_0 \rightarrow {}^5D_0$  region defect spectral lines are studied in further detail, using techniques of nuclear quadrupole optical hole burning, optically detected nuclear quadrupole resonance (ODNQR), and time resolved fluorescence spectroscopy.

## 2. $\text{EuVO}_4$ preparation and description

### 2.1. $\text{EuVO}_4$ crystal preparation

It is appropriate to describe the preparation techniques in some detail, since the observed  $\text{Eu}^{3+}$  spectra are found to be dependent on the method of crystal preparation. Different preparation techniques can affect the purity of the crystals and can give rise to different types and abundances of point defects.

The first crystals studied were prepared using the original technique described by Smith and Wanklyn (1974). The rare earth ion  $\text{Eu}^{3+}$  was introduced into the flux mixture in the form of its oxide, usually 99.9%  $\text{Eu}_2\text{O}_3$ , and placed in a pure platinum crucible. The crucible was then sealed with a tight fitting platinum lid, surrounded by alumina powder, and placed inside an alumina crucible. This helped absorb volatile materials released during the initial stages. It was then heated to an initial soak temperature of 1350°C. This was maintained for around 12 h, at which point a slow cooling would start at a rate of 0.6°C h<sup>-1</sup> until a final temperature of around 930°C was reached. The crucible was then removed and immediately inverted, followed by rapid cooling at around 100°C h<sup>-1</sup>. This resulted in the formation of good quality optically clear crystals near the base of the crucible.

The later crystal growths were prepared using an improved technique described by Wanklyn *et al* (1984). There are several essential differences in this technique compared to the original. The crucible design was changed so that crucibles of double the normal wall thickness with closely fitting lids were used. In addition an inverted inner crucible was used as shown in figure 1. This was packed with the starting materials, as was the base of the outer crucible, then inverted and wedged in place. The outer crucible was subsequently sealed, and the whole assembly placed in the furnace. As the flux melts and evaporates, a layer of crystalline material forms around the join of the inner crucible forming an effective seal and preventing further evaporation; it also prevents elements constantly present in the furnace from contaminating the growth mixture. The initial flux was also changed to incorporate a substantial proportion of  $\text{PbF}_2$ . This was in response to other work (Wanklyn 1977, 1978) indicating that the inclusion of  $\text{PbF}_2$  greatly increases the solubility of the other materials and results in fewer larger crystals. Extensive damage to the platinum crucibles occurred at the previous soak temperature of 1350°C, so this was reduced to 1270°C.

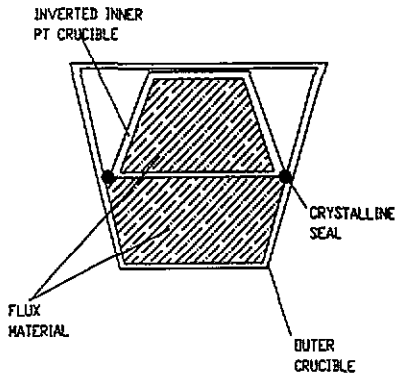


Figure 1. Double platinum crucible arrangement for flux growth of high-purity  $\text{EuVO}_4$  crystals. The inverted inner crucible becomes sealed to the outer by the flux, preventing the entry of contaminants from the furnace.

Later growths used somewhat different starting materials for the flux mixture in an attempt to identify common factors between the flux mixtures used and the final effect on the defect spectrum of the crystals. Some crystals were also grown with other rare earth ions intentionally present in low concentrations. Table 1 gives an overview of the various  $\text{EuVO}_4$  growths used in this study. Each is described further below.

Growth A was a post-1984 growth made from 99.9%  $\text{Eu}_2\text{O}_3$  and a flux containing simply an excess of  $\text{V}_2\text{O}_5$ . The mixture was contained in a new inner and new outer crucible. This was a deliberate effort to make a batch of  $\text{EuVO}_4$  as pure as possible.

Growth B was prepared in a similar manner using even purer starting compounds. The  $\text{Eu}_2\text{O}_3$  was 'specpure'; i.e. at least 99.99% Eu.

Growth C was obtained from IBM Research Laboratories, Yorktown Heights, NY, USA, and had been grown from a pure mixture involving only  $\text{V}_2\text{O}_5$  and 100 ppm  $\text{Gd}^{3+}$ .

Growth D represents the original  $\text{EuVO}_4$  used in the original work by Cone *et al* (1984) and in the comparative study on  $\text{EuAsO}_4$  (Cone *et al* 1988).

Growth E with 1%  $\text{Eu}^{3+}$  in  $\text{GdVO}_4$  was prepared for comparison with  $\text{EuVO}_4$ , as  $\text{Gd}^{3+}$  is next to  $\text{Eu}^{3+}$  in the periodic table, and both ions have very similar ionic radii.  $\text{GdVO}_4$  also undergoes an antiferromagnetic transition at 2.5 K, thereby allowing the possibility of studying the  $\text{Eu}^{3+}$  defect structure in both paramagnetic and magnetically ordered regimes.

Growth F with 10%  $\text{Eu}^{3+}$  in  $\text{YVO}_4$  likewise provided a potentially interesting comparison with stoichiometric  $\text{EuVO}_4$ .

Growth G was designed to maximise the amount of lead and other contaminants taken up in the  $\text{EuVO}_4$  lattice.

Growth H was similar to G except that the crucible, though thoroughly cleaned, was not new, and  $\text{Sm}^{3+}$  was added as a dopant. This was therefore the most contaminated  $\text{EuVO}_4$  growth on the list.

Growth I was the result of an initial flux mixture that did not contain any trace of lead—only KF and  $\text{K}_2\text{O}$ . This was also one of the first growths to use an inner crucible.

Growths J and K were formed in identical fashion to growth I, with the exception of the rare earth dopants  $\text{Ho}^{3+}$  and  $\text{Dy}^{3+}$  respectively.

Growth L used another new flux mixture that did not contain any lead or fluorine contaminants—only excess  $\text{K}_2\text{O}$ . This was however prepared in a single rather than double crucible, and the crucible though cleaned was not brand new. Hence, there is a strong likelihood of external contamination having occurred here, from volatile contaminants always present in the furnace being absorbed in the platinum crucible.

## 2.2. External morphology of the $\text{EuVO}_4$ crystals

The majority of crystals examined were of high optical quality, with no indication of macroscopic defects. Microscopic examination did reveal regions of trapped flux inclusions, though these could easily be avoided during laser excitation experiments. Growths A, I and L were near-colourless transparent crystals, D and G were slightly yellow, while E and H were brown. All crystals were parallelepipeds having typical dimensions  $6 \text{ mm} \times 3 \text{ mm} \times 2 \text{ mm}$ , with the longest dimension parallel to the crystallographic  $c$ -axis and natural faces containing either the  $a$ - $c$  or  $a'$ - $c$  planes.

## 3. Experimental techniques

Optical absorption spectra in the  ${}^7\text{F}_0 \rightarrow {}^5\text{D}_{1,2,3}$  regions were recorded using a 3.4 m Ebert spectrograph with a grating with  $1200 \text{ grooves mm}^{-1}$  and with wavelength calibration being provided by the emission spectrum of an atmospheric iron arc. There were no temperature dependent changes in transition energies in the liquid helium range, and all crystals were always studied while immersed in liquid helium at 1.5 K. Excitation spectra in the  ${}^7\text{F}_0 \rightarrow {}^5\text{D}_0$  range were used to measure weaker absorptions attributed to the intrinsic site and to the various defect sites. The excitation spectra were produced with a Coherent CR599/21 cw laser using Rhodamine-6G dye ( $\sim 580 \text{ nm}$ ); this laser was also used for the hole burning and ODNQR experiments discussed in other papers (Cone *et al* 1992). The excitation spectra were recorded as a function of frequency, with the laser frequency measured using a double Michelson interferometer referenced to an He-Ne laser. Excitation spectra in the  ${}^7\text{F}_0 \rightarrow {}^5\text{D}_{1,2,3}$  regions were produced at Montana State University by a pulsed tunable dye laser system used in conjunction with a 1 m Spex monochromator as described more fully elsewhere (Sun *et al* 1993). Two superconducting magnets were used in this work: a 6 T axial access at Montana State University and a 9 T radial access solenoid at Oxford.

Table 1.

Growth	Flux composition	Comments
A: $\text{EuVO}_4$	$\text{V}_2\text{O}_5$	'Pure'
B: $\text{EuVO}_4$	$\text{V}_2\text{O}_5$	'Superpure'
C: $\text{EuVO}_4$ :0.01% $\text{Gd}^{3+}$	$\text{V}_2\text{O}_5/\text{Gd}_2\text{O}_3$	IBM growth
D: $\text{EuVO}_4$	$\text{Pb}_2\text{V}_2\text{O}_7/\text{V}_2\text{O}_5$	Original growth
E: $\text{GdVO}_4$ :1% $\text{Eu}^{3+}$	$\text{Pb}_2\text{V}_2\text{O}_7/\text{V}_2\text{O}_5$	For comparison
F: $\text{YVO}_4$ :10% $\text{Eu}^{3+}$	$\text{Pb}_2\text{V}_2\text{O}_7/\text{V}_2\text{O}_5$	For comparison
G: $\text{EuVO}_4$	$\text{PbO}/\text{PbF}_2/\text{V}_2\text{O}_5$	Excess Pb
H: $\text{EuVO}_4$ :1.5% $\text{Sm}^{3+}$	$\text{PbO}/\text{PbF}_2/\text{V}_2\text{O}_5/\text{Sm}_2\text{O}_3$	Doped with $\text{Sm}^{3+}$
I: $\text{EuVO}_4$	$\text{KF}/\text{V}_2\text{O}_5$	New flux mixture
J: $\text{EuVO}_4$ :1% $\text{Ho}^{3+}$	$\text{KF}/\text{V}_2\text{O}_5/\text{Ho}_2\text{O}_3$	Doped with $\text{Ho}^{3+}$
K: $\text{EuVO}_4$ :1% $\text{Dy}^{3+}$	$\text{KF}/\text{V}_2\text{O}_5/\text{Dy}_2\text{O}_3$	Doped with $\text{Dy}^{3+}$
L: $\text{EuVO}_4$	$\text{K}_2\text{O}/\text{V}_2\text{O}_5$	New flux mixture

## 4. Intrinsic site spectroscopy

### 4.1. $\text{Eu}^{3+}$ intrinsic site absorption spectra in $\text{EuVO}_4$

These results are discussed first to provide a basis for discussion of the much more complex defect site spectra. Table 2 lists the data obtained from absorption and

emission experiments carried out on growth A (pure)  $\text{EuVO}_4$  crystals. The group theoretical notation given for each transition corresponds to that of the excited state in each case, the ground state  ${}^7F_0$  being  $\Gamma_1$  in the  $D_{2d}$  point group symmetry of the  $\text{Eu}^{3+}$  site in  $\text{EuVO}_4$ . The  $D_{2d}$   $\Gamma_i$  notation is used here because the spectra were all found to obey selection rules and have polarizations consistent with  $D_{2d}$  point symmetry, with some transitions exhibiting mixed magnetic and electric dipole character as noted below.

Table 2.  $\text{Eu}^{3+}$  transition energies in  $\text{EuVO}_4$ : growth A.

Transitions	Energy ( $\text{cm}^{-1}$ )	Differences ( $\text{cm}^{-1}$ )
Absorption		
${}^7F_0 - {}^5D_0$	17196.7 ( $\Gamma_1$ )	0
${}^7F_0 - {}^5D_1$	18953.2 ( $\Gamma_5$ )	3.7
	18949.5 ( $\Gamma_2$ )	0
${}^7F_0 - {}^5D_2$	21469.5 ( $\Gamma_4$ )	89.7
	21435.7 ( $\Gamma_1$ )	55.9
	21414.6 ( $\Gamma_5$ )	34.8
	21379.8 ( $\Gamma_3$ )	0
${}^7F_0 - {}^5D_3$	24317.5 ( $\Gamma_4$ )	57.4
	24312.4 ( $\Gamma_5$ )	52.2
	24271.9 ( $\Gamma_5$ )	11.8
	24271.8 ( $\Gamma_2$ )	11.7
	24260.1 ( $\Gamma_3$ )	0
Emission		
${}^5D_0 - {}^7F_1$	16837.4 ( $\Gamma_2$ )	10.2
	16827.2 ( $\Gamma_5$ )	0
${}^5D_0 - {}^7F_2$	16254.1 ( $\Gamma_4$ )	108
	16146.1 ( $\Gamma_5$ )	0

4.1.1. *Intrinsic site  ${}^7F_0 \rightarrow {}^5D_0$  transition.*  ${}^7F_0 \rightarrow {}^5D_0$  transition, being  $\Gamma_1 \rightarrow \Gamma_1$ , is strictly forbidden in zero magnetic field but exhibits an intensity that varies quadratically with field (see section 6.1). It was found that this transition could just be observed by conventional photographic absorption spectroscopy at the highest field (9 T) for  $B \perp c$  and polarization  $E \parallel c$ , at  $17197 \pm 1 \text{ cm}^{-1}$ . The energy shift of this transition between zero and 9 T is calculated to be very small— $\sim 0.17 \text{ cm}^{-1}$ —so this necessarily less exact determination is therefore in excellent agreement with the more precise value in table 2 obtained from laser excitation spectra in applied magnetic fields.

4.1.2. *Intrinsic site  ${}^7F_0 \rightarrow {}^5D_1$  transitions.* The transition to the  $\Gamma_5$  (doublet) state is found to be polarization independent and therefore of mixed magnetic and electric dipole character, consistent with  $\Delta J = 1$ , while the transition to  $\Gamma_2$  is strongly polarized  $E \perp c$ , indicating that it is of magnetic dipole origin. The effect of magnetic field applied parallel and perpendicular to the  $c$  axis is shown in figure 2. This is a perfect textbook  $J = 1$  Zeeman effect. The  ${}^5D_2$  levels are sufficiently distant in energy that  $J$  mixing effects are negligible. The linear splitting for  $B \parallel c$  yields  $g_J = 1.49 \pm 0.01$ , in excellent agreement with the calculated value of 1.495 from the

heavily intermediate coupled  ${}^5D_1$  wavefunctions given by Ofelt (1963) and our own work (Sun et al 1993). It should be noted that in spite of the complex admixture of states in the intermediate coupled  ${}^5D_1$  wavefunction, the admixtures consist almost entirely of states for which  $L = S$ . In such cases  $g_J = 1.50$  exactly, independent of  $L$  and  $S$ . It is the very small admixture of  ${}^5F_1$  (for which  $L \neq S$ ) that causes the small departure from  $g_J = 1.500$ .

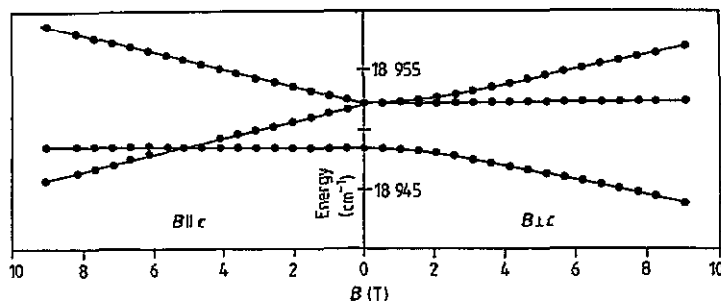


Figure 2. Zeeman effect for the  ${}^7F_0 \rightarrow {}^5D_1$  transition, for magnetic field parallel to the  $a$  and  $c$  axes. The linear doublet splitting for  $B$  parallel to  $c$  corresponds to  $g_J = 1.49 \pm 0.01$ .

4.1.3. *Intrinsic site  ${}^7F_0 \rightarrow {}^5D_2$  transitions.* Of the three singlet states ( $\Gamma_1, \Gamma_3, \Gamma_4$ ) and one doublet state ( $\Gamma_5$ ) expected in  ${}^5D_2$ , transitions in zero applied field are observed only to  $\Gamma_5$  ( $E \perp c$ ) and  $\Gamma_4$  ( $E \parallel c$ ), as expected. Figure 3 shows the energy variation for field applied parallel and perpendicular to  $c$ . In the former case the  $\Gamma_5$  splitting yields  $g_J = 1.46 \pm 0.01$ , which is not in good agreement with the value of 1.492 predicted from the intermediate coupled wavefunctions (Ofelt 1963). It does however agree with the corresponding measurement (Robinson 1986) in the isomorph  $\text{EuAsO}_4$ , and is probably evidence for the small effect to be expected from  $J$  mixing with  ${}^5D_3$ , the nearest level. In the latter case ( $B \perp c$ ) the observation of the remaining transitions in non-zero fields is exactly as expected on symmetry grounds.

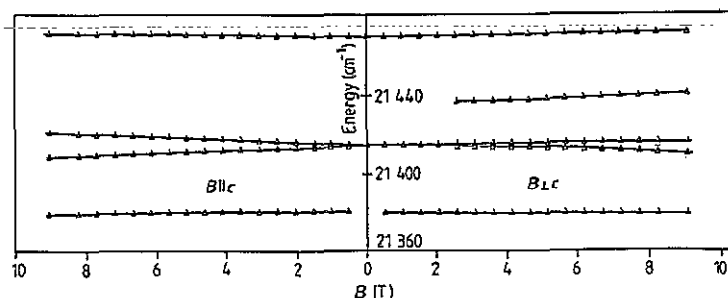


Figure 3. Zeeman effect for the  ${}^7F_0 \rightarrow {}^5D_2$  transition, for magnetic field parallel to the  $a$  and  $c$  axes. The linear doublet splitting for  $B$  parallel to  $c$  corresponds to  $g_J = 1.46 \pm 0.01$  (see text). Only two transitions are observed in zero field.

4.1.4. *Intrinsic site  ${}^7F_0 \rightarrow {}^5D_3$  transitions.* Of the three singlet states ( $\Gamma_2, \Gamma_3, \Gamma_4$ ) and two doublet states ( $\Gamma_5$ ) expected in  ${}^5D_3$ , transitions are observed only to the  $\Gamma_4$  and

$\Gamma_5$  states, as noted for  ${}^5D_2$  above, and with the same polarizations, implying electric dipole behaviour as expected. Quantitative analysis of the  $\Gamma_5$  splittings in-field is more complicated as the two levels are mixed in-field by an amount that depends on all the (crystal field) parameters describing the splittings in  ${}^5D_3$ .

**4.1.5. Fluorescence spectra.** Fluorescence transitions from the long-lived  ${}^5D_0$  state of  $\text{Eu}^{3+}$  are allowed to components of all the  ${}^7F_J$  levels. The transitions to  ${}^7F_1$  and  ${}^7F_2$  are extremely important, as the energy differences  ${}^7F_0$ - ${}^7F_1$  and  ${}^7F_0$ - ${}^7F_2$  almost wholly determine the magnetic properties of the  ${}^7F_0$  ground state. The ground state properties are in turn required for analysis of hole burning and ODNQR spectra in site geometry studies.

Much of this  ${}^5D_0$ - ${}^7F_J$  fluorescence in  $\text{EuVO}_4$  comes from some of the minority of  $\text{Eu}^{3+}$  sites that we refer to as *perturbed* or *defect*  $\text{Eu}^{3+}$  sites; that is, many of these sites are behaving as *fluorescent traps*, and much of any steady state excitation is transferred to them even though they represent a minute fraction of the total  $\text{Eu}^{3+}$  sites. Similar effects were reported for  $\text{EuAsO}_4$  (Cone *et al* 1988). This makes fluorescence spectroscopy quite different from absorption spectroscopy in terms of both the information that it provides and the challenges that it presents.

For  $\text{EuVO}_4$ , the  ${}^5D_0 \rightarrow {}^7F_1$  and  ${}^7F_2$  spectral region contains lines whose energies vary as the excitation is changed from one site to another, but it also contains lines that are always at the same energy regardless of the particular site. These latter lines can be shown to arise from the intrinsic  $\text{Eu}^{3+}$  site  ${}^7F_1$  and  ${}^7F_2$  levels, and the results are given in table 2.

The task of separating the so-called *intrinsic fluorescence*, involving transitions from intrinsic  $\text{Eu}^{3+}$  sites, from the rather similar defect fluorescence has required time resolved spectroscopy with selective laser excitation of individual defect or intrinsic absorption lines. A systematic application of that technique to the determination of both intrinsic and defect site levels in various samples of  $\text{EuVO}_4$  and to the dilute structural isomorphs  $\text{Eu}^{3+}:\text{YVO}_4$  and  $\text{Eu}^{3+}:\text{LuVO}_4$  will be reported elsewhere, along with detailed free ion and crystal field analyses (Sun *et al* 1993). As noted earlier, an unambiguous determination of the energies and electronic wave functions of the  ${}^7F_1$  and  ${}^7F_2$  levels for individual types of defect sites is crucial to detailed interpretation of the site geometry studies carried out via the higher-resolution techniques of spectral hole burning and ODNQR.

**4.1.6. Crystal field analysis.** In the  $D_{2d}$  crystal field Hamiltonian the terms  $B_{kq} C_q^{(k)}$  for  $k = 2, 4, 6$  are important for the  ${}^5D_J$  and  ${}^7F_J$  levels given in table 2. A crystal field analysis is not being discussed here, but it is interesting to note that the very small splittings of the  ${}^7F_1$  and  ${}^5D_1$  levels imply that the important  $B_{20}$  parameter is approximately zero for  $\text{EuVO}_4$ .

## 5. $\text{EuVO}_4$ defect excitation spectra in the ${}^7F_0 \rightarrow {}^5D_0$ region

Since the unperturbed intrinsic sites are in the majority, they dominate the conventional absorption spectroscopy described in section 4. Observation of weaker defect site absorptions on the  ${}^7F_0$  and  ${}^5D_0$  transition, nevertheless, is made straightforward through the method of fluorescence excitation. That technique has high sensitivity since it monitors weak absorption via detection of the resulting fluorescence and is thus nominally a zero-background detection scheme.

### 5.1. Recording the defect maps

All the  $\text{EuVO}_4$  growths listed in table 1 have been examined by the laser excitation technique, producing excitation profiles or *defect maps* in the vicinity of the intrinsic  $^5\text{D}_0 \rightarrow ^7\text{F}_0$  wavelength region. These defect maps plot the defect line fluorescence excitation intensities and line widths as a function of frequency. Growth D was the preparation used in the original work (Cone et al 1984), but for present purposes it was measured anew using refined techniques.

Several additional points should be made about the fluorescence excitation technique. The defect absorptions are weak, so there is no significant distortion of the absorption profiles of individual defect lines. Also, the absolute signal intensity for the same line in the same crystal was repeatable to within a factor of two in different experiments. However, the comparison of relative fluorescent intensities from sample to sample gives variable results, due to inevitable variation in (i) the coupling of the input laser radiation into samples of different shapes and sizes and (ii) the collection of the output fluorescence using fibre optic light guides. In addition, one does not know *a priori* the individual transition probabilities for unidentified defect sites. It is clear therefore that for the results reported here there can be no quantitative comparison between the intensities of individual defect lines from map to map, or between different defect lines in a particular map. Such comparisons remain a practical goal for the future.

For recording of the excitation profiles shown in figures 4 and 5, the crystals were always mounted with the *c* axis vertical, and the laser was polarized  $E||c$ . It was found that although the polarization of the input laser beam had observable effects on the output fluorescence intensity, there was no evidence of complete polarization dependency for any individual defect line. This is consistent with the view that the individual defect site symmetry needs to be low for the transition to be observed at all in zero field. The maps were constructed by recording the excitation spectrum as a series of 30 GHz scans—the maximum scanning range of the continuous wave dye laser. Individual scans were overlapped by 10 GHz, corresponding to one thick etalon mode-hop in the laser scanning system. This procedure was repeated from  $\sim 10 \text{ cm}^{-1}$  below the intrinsic line to  $\sim 50 \text{ cm}^{-1}$  above it; that is, around ninety separate recordings were made and then joined together for each map. Frequency calibration of the spectra was achieved by using the double Michelson wavemeter on all the prominent lines, giving an accuracy of  $\pm 2 \text{ GHz}$ .

Figure 4 shows the maps for each of the  $\text{EuVO}_4$  growths listed in table 1 over the frequency range 515200–517000 GHz ( $\sim 580$ –482 nm), while figure 5 shows the detailed structure in the vicinity of the intrinsic transition, 515450–515590 GHz ( $\sim 581.46$ –581.62 nm).

### 5.2. General comments on the results

Among the different growths, there is a wide range of line widths and intensities for the individual defect lines, but for all growths and for the extended spectral region of figure 4, many of the lines appear to be universally present. This leads to the conclusion that while the spectra differ in detail, a number of the major defect lines appear likely to be a natural characteristic of  $\text{EuVO}_4$  itself rather than the specific crystal growth procedure.

Even samples grown with exceptional regard to purity (A and B) display numerous lines. There is a striking similarity between growths A and C, where in the latter the

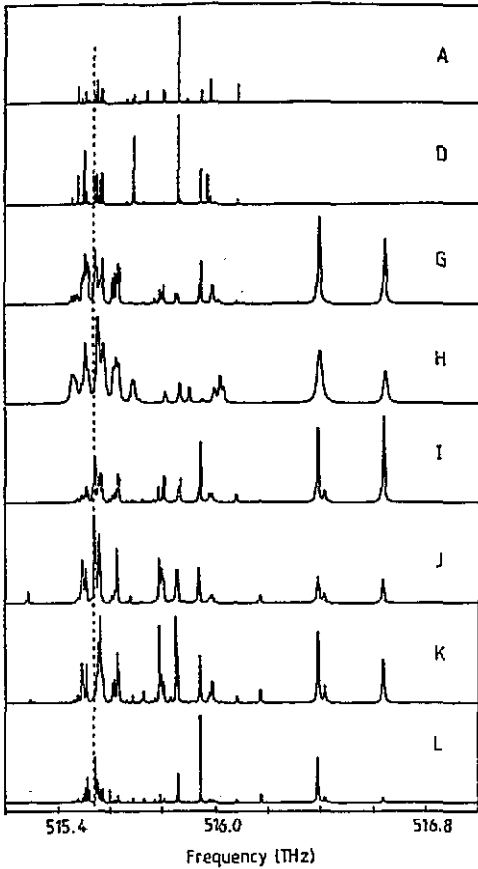


Figure 4. Excitation maps for all  $\text{EuVO}_4$  growths listed in table 1; that is, a plot of integrated fluorescence intensity ( $^5\text{D}_0 \rightarrow ^7\text{F}_1, ^7\text{F}_2$ ) as a function of excitation laser frequency. The dashed line marks the frequency of the intrinsic transition: 515.544 THz ( $17196.7 \text{ cm}^{-1}$ ).

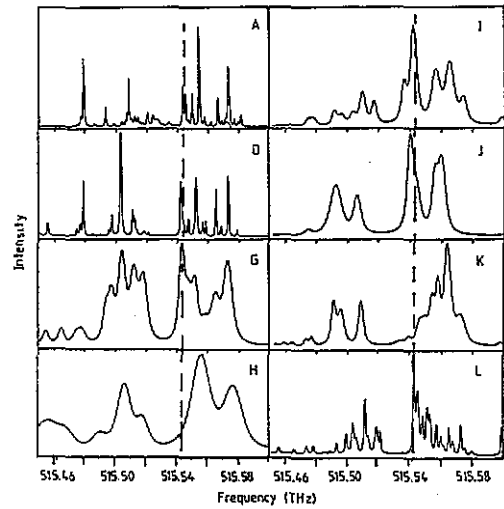


Figure 5. Excitation maps as in figure 4 but only in the vicinity of the intrinsic transition (515.544 THz), which is marked by a dashed line.

100 ppm  $\text{Gd}^{3+}$  dopant is so small an amount that it is equivalent to using 99.99% Eu. These two were grown independently at different laboratories, with no collaboration, yet over this extended spectra region all the lines appear to have identical energies and very similar relative intensities.

Two particularly clear-cut examples of lines that appear universally in the less pure growths are two of the highest energy lines at  $\sim 516389$  and  $516635$  GHz, with the former appearing as two lines in some growths. These lines appear to be strong in all the growths where fluorine was present in the flux used in the growth process. The same lines do appear in growth L, where no fluorine was used in the flux, but as already noted in section 2, there is circumstantial evidence that contamination of the melt could have occurred in that case.

### 5.3. Search for possible contaminants by other techniques

In a search for possible contaminants that might be present in the crystals, samples from growths D and G were analysed by mass spectrometry at Oak Ridge National

Laboratory (Abraham 1992). Unfortunately the technique was not able to identify fluorine, but lead was found at 1000 ppm in growth D and 1300 ppm in growth G where lead based fluxes had been used. EPR measurements, also carried out at Oak Ridge, showed the presence of  $Gd^{3+}$ —always expected as a contaminant in compounds of europium—but showed no paramagnetic  $Pb^{3+}$ , so the lead is presumably either divalent or quadravalent in these  $EuVO_4$  crystals. Growth H (1.5%  $Sm^{3+}$ ) crystals were examined for (ferromagnetic) iron content using the SQUID magnetometry facility in the Department of Earth Sciences, Oxford University; this gave an iron concentration no more than 1 in  $10^{10}$ . The results for lead suggest that it is an important contaminant, yet with the high measured concentrations found for growths D and G, the corresponding maps may be taken as an indication that lead is surprisingly unimportant in producing many of the observed defect sites. Figure 5 shows, for example, that the lines for G are very much broader than those for D, but that is unlikely to be due to a mere 30% increase in lead content. Some other factor must have been responsible for the very large line widths in the spectrum for growth G.

#### 5.4. Effects of annealing and irradiation

To investigate possible effects due to local structural disorders, stressed regions, vacancies, and dislocations, several  $EuVO_4$  crystals, especially from growth A (pure) were annealed at high temperature (1350 °C) and re-mapped. There were very slight changes in the physical appearance of the crystals, but no changes in the excitation maps. The possibility of simple colour centres—unlikely, since there are no reports in the literature of colour centres being observed in any rare earth vanadate, phosphate, or arsenate crystals—was investigated by irradiating several crystals in an intense x-ray source ( $5 \text{ krad min}^{-1}$ ). Again, there were no changes evident in the excitation maps.

#### 5.5. Discussion of spectral shifts and distributions

In addition to the sheer number of defect sites evident in the excitation maps, one must wonder at the wide distribution of site energies. The site dependent energy shifts cannot be explained by the crystal field alone. If, for example, the crystal field parameters for the intrinsic site are set to zero, keeping all free ion parameters the same, the  ${}^5D_0 \rightarrow {}^7F_0$  transition energy shifts by only  $\sim 30 \text{ GHz}$ . Even if one imagines strongly distorted sites with much greater crystal fields than the intrinsic sites, it is unreasonable to attribute the total energy spread of  $1800 \text{ GHz}$  ( $60 \text{ cm}^{-1}$ ) to changes in the crystal field arising from local distortions. Local perturbations of the ionic environment need to alter the free ion energies through the Slater parameters, for example, in order to produce the observed effects.

The region immediately surrounding the intrinsic site energy is highlighted in figure 5. Apart from accidental degeneracies, lines very close (less than  $\sim 30 \text{ GHz}$ ) to the intrinsic site energy can be regarded as 'minimally' perturbed; that is, they represent sites which are in some way removed from the physical perturbation and consequently are relatively shielded from it. One might argue that there must be a very large number of such minimally perturbed sites, perhaps three or more unit cells away from the site of each point defect. For a random distribution of defects in the lattice this would lead to the expectation that there should be a Gaussian envelope of inhomogeneously broadened minimally perturbed sites around the intrinsic energy, visible as one broad line. The fact that this is not seen must indicate that there is a limit to how minimally perturbed an individual site can be. Thus,  $Eu^{3+}$  ions well

away from the perturbation site seem to be effectively fully shielded from experiencing any perturbation. Closer than this, there can only be a few shells, perhaps within a radius of only two or three unit cells, where the  $\text{Eu}^{3+}$  ions experience a perturbation large enough to have an effect on the electronic energy—and yet small enough to be described by perturbation theory.

On most of the maps there is an energy 'gap' 20–30 GHz wide just below the intrinsic line position. (The intrinsic line position was determined by experiments using applied magnetic field, as discussed in the next section.) This can, perhaps, be taken as evidence that the original lattice structure is 'good' in the sense that minor local distortions of the structure do not produce a state of lower energy. It may also be significant that this gap is comparable with the effect of the crystal field on the  ${}^7\text{F}_0 \rightarrow {}^5\text{D}_0$  transition. Perhaps more important, however, is the observation from figure 5 that few if any of the lines in the vicinity of the intrinsic transition are truly universal amongst the various growths.

### 5.6. Attribution of specific $\text{Eu}^{3+}$ defect sites in other systems

There has been extensive work on optical studies of  $\text{Eu}^{3+}$  in host compounds as reviewed by Morrison and Leavitt (1982) and Macfarlane and Shelby (1987). Site selective spectroscopy has been employed by Venikouas and Powell (1978) for  $\text{Eu}^{3+}$  in  $\text{YVO}_4$ , but there has been no other work on defect sites in the vanadate or arsenate systems.

The  $\text{Eu}^{3+}$  doped ionic halide lattices such as  $\text{SrF}_2:\text{Eu}^{3+}$  (Jouart *et al* 1985),  $\text{SrCl}_2:\text{Eu}^{3+}$  (Wietfeldt and Wright 1985, 1987),  $\text{BaF}_2:\text{Eu}^{3+}$  (Jouart *et al* 1987) and  $\text{PbF}_2:\text{Eu}^{3+}$  (Weesner *et al* 1986) have been studied by various techniques including site selective laser spectroscopy, and analysis of the electronic selection rules and optical polarization has allowed the identification of defect site symmetry in several cases. In those cases, a specific charge compensated defect site is prevalent. The precision techniques of hole burning and ODNQR have been used to confirm such an interpretation for  $\text{CaF}_2:\text{Eu}^{3+}$  and  $\text{CdF}_2:\text{Eu}^{3+}$  (Silversmith *et al* 1986).

Although the present work employs similar experimental techniques, the absence of clear polarization and/or selection rule behaviour for the defect site optical transitions in  $\text{EuVO}_4$  means that the problem of individual site identification in these crystals is more difficult, and is still at a very early stage. However, knowing that the crystals almost certainly contain lead, and that some contain fluorine as well, various possible defect sites suggest themselves.  $\text{Pb}^{n+}$  in a rare earth, vanadium or interstitial site, with charge compensation provided locally by  $\text{F}^-$  as necessary, are obvious possibilities. Cone *et al* (1992, 1993) begin to address such matters, but with such a large number of defect lines, all by definition related to  $\text{Eu}^{3+}$  sites of low symmetry, the relation between any individual defect line and a detailed description of the corresponding defect site has not been achieved yet.

### 5.7. Defect line shape analysis

The line shapes of several of the prominent lines were found to be very well described by Voigt profiles, i.e. convolutions of Lorentzian and Gaussian contributions; however, this is not thought to have obvious physical significance, as the fitted Lorentzian contributions (typically  $\sim 1$  GHz) are very much larger than the limits on homogeneous widths of several MHz implied by hole burning experiments (discussed in Cone *et al* 1984, 1992, 1993).

## 6. Zeeman effects and inequivalence splittings

### 6.1. Intrinsic site enhancement and Zeeman shifts

Both  ${}^7F_0$  and  ${}^5D_0$  are non-magnetic  $J = 0$  states, leading to a quadratic field dependence of their energies that arises out of admixtures of  ${}^7F_1$  and  ${}^5D_1$  states respectively through matrix elements of the Zeeman Hamiltonian

$$H = \mu_B(L + 2S) \cdot B.$$

Another consequence of this admixture is that the  ${}^7F_0 \rightarrow {}^5D_0$  transition, which is strictly forbidden and therefore of zero intensity at the intrinsic site, becomes progressively allowed in a magnetic field, with an intensity that should increase as  $B^2$ . Indeed, this field dependence is essential to the identification of the intrinsic line position, as it always appears to originate at the same energy ( $17196.7 \text{ cm}^{-1}$ , see table 2) in all  $\text{EuVO}_4$  crystals and can be observed only in non-zero field. The intrinsic line intensity has been measured as a function of applied field for all crystal growths, and is found to be accurately quadratic with field. Because there is always a non-zero fluorescence intensity at the intrinsic line position in these samples, even in zero field, the intensity enhancement relative to this baseline varies greatly, being largest (a factor of  $\sim 350$  at 8 T) for the very pure growth A, and smallest (a factor of  $\sim 4$  at 8 T) for the 'dirty' growths G and H.

In contrast to this *qualitative* prediction concerning dependence of intensity on field, an important *quantitative* prediction can be made regarding the *energy* dependence of the intrinsic site line on field. From second-order perturbation theory, the expected shift in the energy of the ground state is calculable for fields along the  $a$  and  $c$  axes, knowing the energy separation between  ${}^7F_0$  and the states  $M_J = \pm 1$  and 0 respectively in  ${}^7F_1$ . The calculation is straightforward because even in intermediate coupling the  $\text{Eu}^{3+}$  ground state is accurately  ${}^7F_0$ . The corresponding calculation for the energy shift in  ${}^5D_0$  is far more tedious due to the appreciable intermediate coupling in all the  ${}^5D$  states. The results are:

$$B \parallel c: \quad \Delta E({}^7F_0 \rightarrow {}^5D_0) = 63.0 B^2 \text{MHz T}^{-2}$$

$$B \perp c: \quad \Delta E({}^7F_0 \rightarrow {}^5D_0) = 61.4 B^2 \text{MHz T}^{-2}$$

Experimentally the  $B^2$  coefficients are found to be  $60 \pm 2 \text{ MHz T}^{-2}$  and  $63 \pm 2 \text{ MHz T}^{-2}$  respectively. Within experimental error both of these values agree with the predictions of the theory. The very similar values are a direct result of the unusually small  ${}^7F_1$  splitting at the intrinsic site.

### 6.2. Inequivalence splittings for defect sites

The  $D_{2d}$  point symmetry at the *intrinsic*  $\text{Eu}^{3+}$  sites in  $\text{EuVO}_4$  implies that the value of any physical property measured with magnetic field parallel to the crystallographic  $a$  axis will be identical to that measured with field parallel to  $a'$ . At  $\text{Eu}^{3+}$  *defect* sites the symmetry is lower, so that for a particular defect site, measurements for field parallel to  $a$  and  $a'$  may well give different values,  $\alpha$  and  $\alpha'$ , say, for some physical property. The consequence of this, in an experiment where one is necessarily looking simultaneously at all sites of a particular type in the  $\text{EuVO}_4$  crystal, is that it is overwhelmingly probable that both values  $\alpha$ ,  $\alpha'$  will be observed along either  $a$  or

$a'$ . That is, there will be as many defect sites of a particular kind related in some fashion to the  $a$  axis as there are related to the  $a'$  axis.

This means for defect sites that there are two magnetically inequivalent  $\text{Eu}^{3+}$  sites for field applied in a general direction in the  $a, a'$  basal plane. In the present experiments, it was possible to apply field only along  $a$  or  $a'$ , but even in this case, inequivalence is expected unless the particular defect site under study happens to have principal axes at  $45^\circ$  to  $a$  or  $a'$ .

All the  ${}^5\text{D}_0 \rightarrow {}^7\text{F}_0$  defect lines for growth A crystals were examined for such inequivalence splittings. That is, the expected quadratic energy variation with field for each line ( $J = 0 \rightarrow J = 0$ ) was examined for signs of line splitting, particularly at the highest field (9 T). Nine lines at the higher-energy end of the excitation spectra displayed well resolved splittings, which were typically  $\sim 5$  GHz at 9 T. Figure 6 shows two typical results, from which it can be seen that the splittings are well resolved, and that the quadratic energy variation is accurately reproduced.

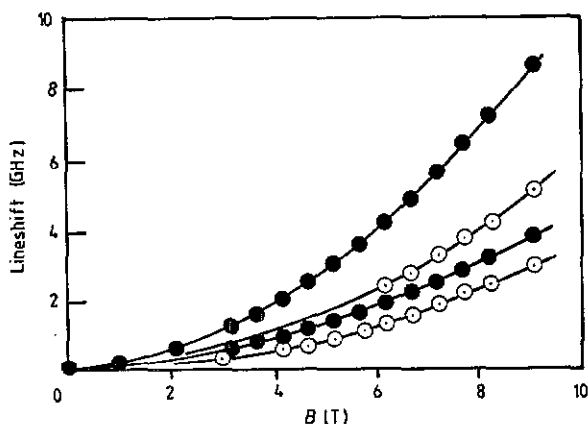


Figure 6. Inequivalence splitting of line 42 (open circles) and line 44 (solid circles) as a function of field applied parallel to the  $a$  axis.

Such data is direct evidence that the principal axes of quantization for each of these nine defect sites are *not* at  $45^\circ$  to  $a, a'$ , with the third axis almost certainly not along  $c$  either (thereby leading to low site symmetry). Ideally all the necessary information concerning the direction of such axes relative to the original  $a, a', c$  axes could be obtained by measuring the inequivalence splitting at constant field, as a function of field direction in the  $a, a'$  plane, and in the planes containing  $c$  and the principal directions in  $a, a'$ . Such experiments are difficult due to the poorer fluorescence detection geometry inevitable when using crystal rotation devices. However, in the absence of such detailed information, the present inequivalence splitting data do allow some conclusions to be drawn concerning the crystal field effects in  ${}^7\text{F}_1$  due to defect site distortion.

In the general case a defect site would display  $C_1$  symmetry; that is, no symmetry at all. A consequence of this would be that relative to any system of local axes  $x, y, z$ , the three crystal field eigenfunctions in  ${}^7\text{F}_1$  would consist of an arbitrary admixture of the three functions  $m_J = |0\rangle, |\pm 1\rangle$  originally described relative to the  $a, a', c$  axes in  $D_{2d}$ . There is little point in proceeding with a general analysis along these lines, given the small amount of experimental data typified by that shown in figure 6. Instead, we argue for an extremum result, based on the simplest possible model of a distorted (defect) site.

In  $D_{2d}$  symmetry the  ${}^7\text{F}_1$  level is split into a  $\Gamma_5$  doublet and a  $\Gamma_2$  singlet, as

shown in table 2. Let us suppose that the lowered symmetry at a particular type of defect site consists of the simplest type of orthorhombic distortion; that is, a local increase of NN atomic distance along the  $a$  axis relative to that along  $a'$ . Because of the overall crystal symmetry we would expect an equal number of such sites in which the local increase was along  $a'$  rather than  $a$ . Relative to the local (orthorhombic symmetry) axes  $a$ ,  $a'$ ,  $c$ , the resulting electronic eigenfunctions would be of the form

$$|1, 0\rangle, (1/\sqrt{2})(|1, +1\rangle + |1, -1\rangle) \quad (1/\sqrt{2})(|1, +1\rangle - |1, -1\rangle)$$

that is,

$$|1, 0\rangle, |1, 1\rangle_s, |1, 1\rangle_a.$$

In the presence of a magnetic field parallel to the  $a$  axis, the Zeeman Hamiltonian would couple the ground state  $|0, 0\rangle$  with  $|1, 1\rangle_s$  for the sites with distortion along  $a$ , and  $|1, 1\rangle_a$  for the sites with distortion along  $a'$ . That is, we need to consider matrix elements of the operators  $(L_x + 2S_x)$  and  $(L_y + 2S_y)$  respectively, and the individual quadratic energy variations with field of these two transitions are given by  $25.15 B^2/\Delta_s$  and  $25.15 B^2/\Delta_a$  GHz T<sup>-2</sup>. These two differ because of the  $\Gamma_5$  splitting ( $\Delta_s - \Delta_a$ ) produced by the local distortion. This model provides a qualitative explanation for the data shown in figure 6.

The important point here is that the above model is the extreme case: any further symmetry-lowering distortion (which would produce further admixture of all three  $J = 1$  eigenfunctions) or any rotation of the local distortion axes away from the magnetic field direction would serve only to *reduce* the observed difference in the quadratic energy variation; that is, the inequivalence splitting. Data of the type shown in figure 6 therefore allow calculation of the *smallest possible* value of  $\Delta_s - \Delta_a$ ; the true values are almost certainly larger. Table 3 lists the results, and shows a large range in the difference  $\Delta_s - \Delta_a$ , as may be expected for quite severe local distortion at particular sites.

Such large splittings are not unprecedented; the G1 Eu<sup>3+</sup> site in CaF<sub>2</sub>:Eu<sup>3+</sup> (Silversmith and Radlinskii 1985) is very similar. More precise values will have to await a determination of local axes. Again it is unfortunate that experimental difficulties have temporarily precluded the direct spectroscopic determination of these splittings in the <sup>7</sup>F<sub>1</sub> manifolds.

The fact that only nine lines display inequivalence splittings, or rather that some eighty percent of the lines do *not* display such behaviour, is almost certainly because the large majority of defect sites have very low symmetry. This tends to produce arbitrary eigenfunction admixture and principal axes directions that tend to mask clear-cut behaviour of the type shown in figure 6.

Table 3.

Line No	Energy (GHz)	$\Delta_s$	$\Delta_a$	$\Delta_s - \Delta_a$
35	515 695	452	367	85
38	515 745	565	371	194
39	515 808	484	388	96
40	515 811	508	372	136
41	515 865	505	357	148
42	515 897	695	399	296
43	515 947	543	239	304
44	515 980	520	197	323
45	516 082	556	382	174
Intrinsic line		372.7	372.7	0.0

### 6.3. Other field dependent lines

As already discussed, the  ${}^7F_0 \rightarrow {}^5D_0$  intrinsic line at  $17\,196.7\text{ cm}^{-1}$  is found for all crystal growths by scanning through the excitation spectrum both with and without magnetic field applied along the  $c$  axis. In the presence of field, for all growths except A there was always just one additional line, always at the same energy:  $17\,196.7\text{ cm}^{-1}$  (515 544 GHz). For growth A, however, there were three other lines that were enhanced in intensity as field was applied. These were line 3 (515 479 GHz), line 14 (515 520 GHz) and line 15 (515 523 GHz). All three lie below the energy of the intrinsic line, and (to be discussed in Cone *et al* 1993) none showed hole burning effects.

All defect  ${}^7F_0 \rightarrow {}^5D_0$  lines are subject to the same quantum mechanical admixture of the  ${}^7F_0$  ground state with the  ${}^7F_1|m_J = 0\rangle$  state that enhances the intrinsic line, but for defect lines the enhancement of intensity is negligible because the lines are already allowed due to the lowered site symmetry. The fact that these three lines can be enhanced—a factor of  $\sim 10$  for lines 3 and 15, and a factor of  $\sim 100$  for 14—therefore indicates that the site symmetry for each must be very high; that is, they must be very nearly  $D_{2d}$  sites. Their clear separation from the true intrinsic line position is somewhat surprising, and certainly relevant to a discussion of crystal field and free ion effects as given in section 5.5 above. That is, the shift from the intrinsic line position in these three cases is almost certainly due to changes in free ion parameters rather than local distortions. This anomalous behaviour singles them out for future detailed studies.

## 7. Experiments on doped crystals: growths E, F, H, J, K

Figures 4 and 5 show that for these growths, which contain either small  $\text{Eu}^{3+}$  concentrations in  $\text{GdVO}_4$  and  $\text{YVO}_4$ , or small  $\text{Sm}^{3+}$ ,  $\text{Ho}^{3+}$ , or  $\text{Dy}^{3+}$  concentrations in  $\text{EuVO}_4$ , the  $\text{Eu}^{3+}$  excitation spectra display the same features as the stoichiometric growths. Spectral line widths are however much larger, to the extent that much of the detail observed in pure  $\text{EuVO}_4$  is lost. In addition, the presence of paramagnetic ions in growths E, H, J, K meant that the lines could not be hole burned, due doubtless to the possibility for enhanced  $\text{Eu}^{3+}$  nuclear spin–lattice relaxation rates.

In growth E (1%  $\text{Eu}^{3+}:\text{GdVO}_4$ ) the spectra were studied at temperatures above and below the antiferromagnetic transition in  $\text{GdVO}_4$ ,  $T_N = 2.495\text{ K}$ , but no changes in the excitation spectrum attributable to magnetic order were observed. For growth H (1.5%  $\text{Sm}^{3+}:\text{EuVO}_4$ ) the existence of a  $1\text{ cm}^{-1}$  zero-field splitting in the  $\Gamma_5$  doublet in  ${}^5D_1$  showed that the crystal was quite severely strained. In addition, the value of  $g_J$  for this doublet was found to be  $1.431 \pm 0.005$ , which is significantly smaller than the  $1.49 \pm 0.01$  found in pure  $\text{EuVO}_4$ , and almost certainly due to a distortion of the site axes rather than a real change in  $g_J$ . For growth J (1%  $\text{Ho}^{3+}:\text{EuVO}_4$ ) a study of the  $\text{Ho}^{3+}$  spectrum has shed valuable light on the spectroscopic properties of the stoichiometric isomorph  $\text{HoVO}_4$ . That work has been published elsewhere (Bleaney *et al* 1988).

## 8. Conclusions

An extensive survey of  $\text{Eu}^{3+}$  defect spectra in the  ${}^7F_0 \rightarrow {}^5D_0$  region has shown that the main features of the defect spectra are largely independent of the method of  $\text{EuVO}_4$  crystal preparation. Even in the purest crystals available there are still some fifty individual lines, which implies a surprisingly large number of different defect

types for so simple a crystal structure. In detail, the defect spectra *are* dependent on the method of crystal preparation, and in particular the presence of fluorine in the growth flux appears to be responsible for several prominent lines at the highest energy. The identification of individual defect sites in this system is still in its infancy, and this work represents no more than the essential first step in the investigation.

The spectroscopic properties of the  $\text{Eu}^{3+}$  ion at the  $D_{2d}$  *intrinsic* sites are well understood. A crystal field analysis of the levels observed in the multiplets  ${}^7F_1$ ,  ${}^5D_1$  leads to the surprising result that the crystal field parameter  $B_{20}$ , responsible for the magnetically important splittings in  ${}^7F_1$ ,  ${}^5D_1$ , is very nearly zero. This has important implications for the quadrupole splittings expected for  $\text{Eu}^{3+}$  at the intrinsic sites, and for the possibility of hole burning and ODNQR experiments, which observe such splittings directly.

### Acknowledgments

The authors would like to thank Dr M M Abraham, Oak Ridge National Laboratory, Oak Ridge, TN, USA, for the trace element analysis of some of the  $\text{EuVO}_4$  crystals, Dr B E Watts for preparing some of the crystal growths, and Y Sun for useful discussions. This research was supported in part by the Science and Engineering Research Council of the UK, NATO Collaborative Research Grant CRG 910031, The Research Corporation, and NSF/EPSCOR (MONTs), and Montana Space Grant Consortium (NASA grant number NGT40041).

### References

- Abraham M M 1992 private communication  
 Bleaney B, Gregg J F, Hansen P C, Huan C H A, Lazzouni M, Leask M J M, Morris I D and Wells M R 1988 *Proc. R. Soc. A* **416** 6  
 Cone R L, Hansen P C and Leask M J M 1992 *J. Opt. Soc. Am.* **9** 779  
 — 1993 to be published  
 Cone R L, Harley R T and Leask M J M 1984 *J. Phys. C: Solid State Phys.* **17** 3101  
 Cone R L, Leask M J M, Robinson M G and Watts B E 1988 *J. Phys. C: Solid State Phys.* **21** 3361  
 Jouart J P, Bissieux C and Mary G 1987 *J. Lumin.* **37** 159  
 Jouart J P, Bissieux C, Mary G and Egee M 1985 *J. Phys. C: Solid State Phys.* **18** 1539  
 Macfarlane R M and Shelby R M 1987 *Spectroscopy of Solids Containing Rare Earth Ions* ed A A Kaplyanski and R M Macfarlane (Amsterdam: North-Holland) pp 51–184  
 Morrison C A and Leavitt R P 1982 *Handbook on the Physics and Chemistry of Rare Earths* vol 5 (Amsterdam: North-Holland)  
 Ofelt G S 1963 *J. Chem. Phys.* **38** 2171  
 Robinson M G 1986 *D. Phil. Thesis* Oxford University  
 Silversmith A J and Radlinskii A P 1985 *J. Phys. C: Solid State Phys.* **18** 4385  
 Silversmith A J, Radlinskii A P and Manson N B 1986 *Phys. Rev. B* **34** 7554  
 Smith S H and Wanklyn B M 1974 *J. Cryst. Growth* **21** 23  
 Sun Y, Cone R L, Leask M J M and Abraham M M 1993 to be published  
 Venikouas G E and Powell R C 1978 *Phys. Rev. B* **17** 3456  
 Wanklyn B M 1977 *J. Cryst. Growth* **37** 334  
 — 1978 *J. Cryst. Growth* **43** 336  
 Wanklyn B M, Watts B E and Garrard B J 1984 *Mater. Res. Bull.* **19** 825  
 Wechsner F J, Wright J C and Fontanella J J 1986 *Phys. Rev. B* **33** 1372  
 Wietfeldt J R and Wright J C 1985 *J. Chem. Phys.* **83** 4210  
 — 1987 *J. Chem. Phys.* **86** 400